

Cavitation bubble nucleation induced by shock-bubble interaction in a gelatin gelRyota Oguri¹ and Keita Ando^{1, a)}*Department of Mechanical Engineering, Keio University, 3-14-1 Hiyoshi Kohoku-ku,
Yokohama 223-8522, Japan*

An optical visualization technique is developed to study cavitation bubble nucleation that results from interaction between a laser-induced shock and a preexisting gas bubble in a 10 wt% gelatin gel; images of the nucleated cavitation bubbles are captured and the cavitation inception pressure is determined based on Euler flow simulation. A spherical gas cavity is generated by focusing an infrared laser pulse into a gas-supersaturated gel and the size of the laser-generated bubble in mechanical equilibrium is tuned via mass transfer of the dissolved gas into the bubble. A spherical shock is then generated, through rapid expansion of plasma induced by the laser focusing, in the vicinity of the gas bubble. The shock-bubble interaction is recorded by a CCD camera with flash illumination of a nanosecond green laser pulse. The observation captures cavitation inception in the gel under tension that results from acoustic impedance mismatching at the bubble interface interacting with the shock. We measure the probability of cavitation inception from a series of the repeated experiments, with varying the bubble radius and the standoff distance. The threshold pressure is defined at the cavitation inception probability equal to one half and is calculated, through comparisons to Euler flow simulation, at -24.4 MPa. This threshold value is similar to that from shock-bubble interaction experiments using water, meaning that viscoelasticity of the 10 wt% gelatin gel has a limited impact on bubble nucleation dynamics.

Keywords: Laser-induced phenomena, Shock-bubble interaction, Cavitation bubble nucleation, Cavitation inception pressure

^{a)}Electronic mail: kando@mech.keio.ac.jp

INTRODUCTION

Acoustic cavitation plays an important role in medical therapy using shockwave and ultrasound; one of the representative examples is shockwave lithotripsy, which is a technique to break kidney stones. In this technique, shockwave is focused extracorporeally to the vicinity of kidney stones and acoustically-triggered cavitation bubbles are believed to promote stone fragmentation via its mechanical action.¹⁻⁴ Another example is that ultrasound-induced cavitation bubbles are used for tissue ablation through their effective heat deposition.^{5,6} However, cavitation bubble dynamics may give rise to side effects such as the rupture of blood vessels.^{7,8} To further improve these medical treatments that rely on acoustic cavitation, it is essential to measure the cavitation inception pressure in (viscoelastic) human tissues. While a number of experiments have been performed to measure cavitation thresholds for (Newtonian) liquids such as water⁹, the measurement for viscoelastic media is yet limited. Ultrasound-induced cavitation in viscoelastic media was reported in recent experimental studies.¹⁰⁻¹²

We now put a focus on cavitation inception that results from shock-bubble interaction.¹³⁻¹⁵ Underwater shockwave interacts with air-water interfaces such as bubbles and reflects as a tension wave due to acoustic impedance mismatching; this tension may in principle induce cavitation bubble nucleation. Ando, Liu, and Ohl¹⁶ developed an optical visualization system to observe underwater shock events with nanosecond laser pulses and studied cavitation bubble nucleation that results from interaction between laser-induced shocks and air-water interfaces in a microchannel. Quinto-Su and Ando¹⁷ observed cavitation bubble nucleation resulting from interaction of a couple of laser-induced shocks and bubbles in pure water and showed, with the aid of Euler flow simulation, that the cavitation inception pressure of ultrapure water is predicted at -20.1 ± 3.4 MPa. However, to the authors' knowledge, cavitation inception caused by shock-bubble interaction in viscoelastic media has not been studied quantitatively.

In this study, we apply the shock-bubble-interaction technique¹⁷ in order to study cavitation inception in a gelatin gel (as a tissue-mimicking phantom), with the aid of Euler flow simulation; the intent is to see effects of the gel viscoelasticity on cavitation inception. Shock-bubble interaction is experimentally realized by focusing a nanosecond laser pulse (at 1064 nm) into a gel (where a gas bubble preexists) and the subsequent cavitation inception is recorded by stroboscopic photography with backlighting of a nanosecond laser pulse (at 532 nm). The probability of cavitation inception is obtained from a series of the repeated experiments. The Euler flow simulation that replicates

The measured shock and bubble evolution is performed to obtain the pressure field. Cavitation inception pressure in the gel is then determined from comparisons between the experiment and the simulation.

II. EXPERIMENT

A. Preparation of gelatin gels

A gelatin gel is used as a tissue-mimicking phantom and made by mixing 10 wt% gelatin (Type-A, Sigma Aldrich) with deionized water. The acoustic impedance of the 10 wt% gelatin gel is similar to that of human arteries, blood, liver, kidney, and other organs.¹⁸ The solution is poured into a cylindrical dish (polystyrene) of 56 mm diameter and 16 mm height. The solution is stored in refrigeration at 4 °C overnight and then placed in room temperature for two hours to return to room temperature before the shock-bubble interaction experiment. Since the mass diffusion of dissolved air in the gel is very gradual in comparison to the heat diffusion, the gel becomes supersaturated with the dissolved gas.¹⁹ Spherical indentation testing (SOFTMEASURE HG1003, HORIGUCHI) was performed to measure Young's modulus E of the gel; our measurement gave $E = 60$ kPa. We note that the value of E at an extremely high strain rate of shock loading (as in the present experiment) is unavailable and can be larger than the measurement of the (quasistatic) indentation testing.²⁰

B. Optical setup for observation of laser-induced phenomena

The schematic of the optical system for observation of laser-induced phenomena is presented in Fig. 1(a). A Q-switched Nd:YAG laser (ULTRA 50 GRM, Quantel) emits single laser pulses simultaneously at wavelengths of 532 nm (green) and 1064 nm (infrared or IR); both laser pulses have 6-ns duration. The IR laser pulse of 1.40 ± 0.01 mJ (where the \pm sign denotes a standard deviation from 10 measurements) is focused into the gel through a microscope objective (40 \times , NA = 0.6). In the focal spot, plasma appears and its rapid expansion produces a spherical shock wave that propagates outward.²¹ Heat deposition after the plasma recombination leads to the formation of a vapor bubble behind the shock. Images (from top view) of the laser-induced phenomena (including shock-bubble interaction and the subsequent cavitation inception) in the gel are captured using a CCD camera (Pixelfly, PCO; one pixel = 0.33 μ m) with stroboscopic

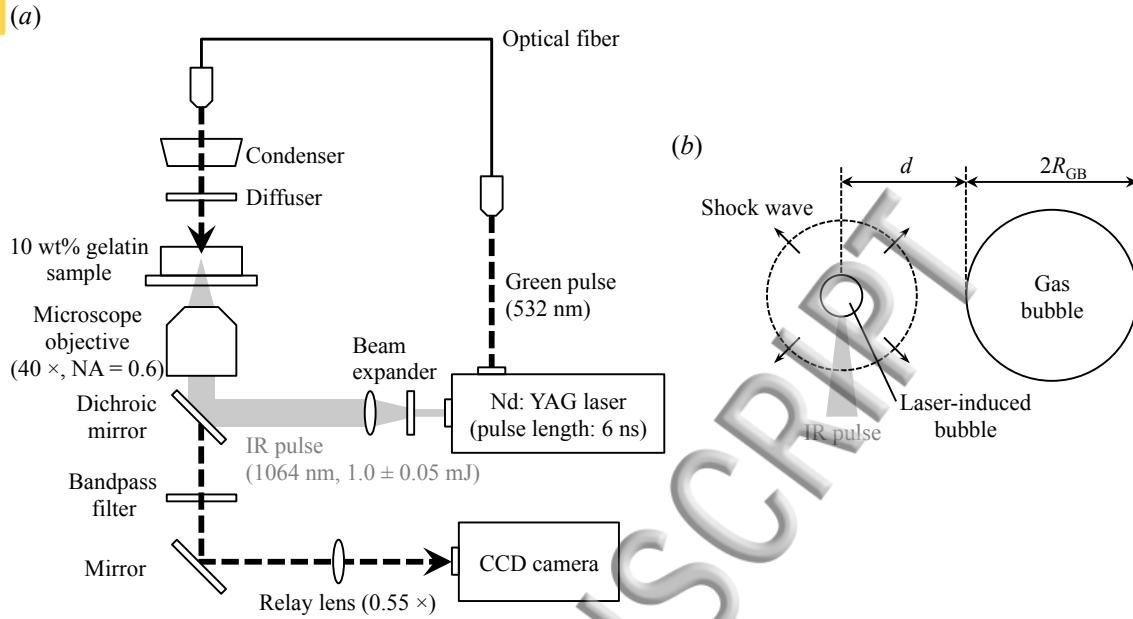


FIG. 1. (a) The optical system for visualization of laser-induced phenomena in the gelatin gel. (b) Illustration of the shock-bubble interaction (side view).

backlighting of the green laser pulse. The illumination timing is tuned by changing the length of the multi-mode optical fiber (F-MFC-OPT High Power Density Step Index Fiber, NA = 0.22, Newport) through which the green laser pulse propagates. Temporal resolution with the 1-m optical fiber is 5 ns. With this setup, we obtain a single image of laser-induced phenomena for each experimental operation (with the given fiber length).

C. Visualization of the laser-induced phenomena without bubble interaction

Before studying shock-bubble interaction in the gel, we first examine the evolution of the laser-induced shock wave and bubble in the gel (without bubbles inside). To avoid wave reflections from the container wall and gel surface, the IR laser pulse is focused sufficiently away from any boundaries. The green laser illumination time is set 13 ns to 78 ns, with 5-ns interval, after the laser focusing, which allows for constructing the evolution of the laser-induced shock and bubble. The visualization is repeated ten times for each illumination time. The constructed evolution of the shock and bubble is used to tune the initial conditions for Euler flow simulation as will be explained in section III B.

Visualization of shock-bubble interaction and the subsequent cavitation inception

A spherical gas bubble (to collide with the laser-induced shock) is created by focusing the IR laser pulse through microscope objective into the (gas-supersaturated) gel. After vapor condenses back into the surrounding medium, a non-condensable air cavity is left.²² The gas bubble (in mechanical equilibrium) grows gradually via mass transfer of the dissolved gas into the bubble, for the gel is gas-supersaturated. The equilibrium radius of the (preexisting) gas bubble is controlled based on the mass diffusion. The IR laser pulse is then shot in the vicinity of the gas bubble so as to realize shock-bubble interaction (Fig. 1(b)). The experimental parameters are:

- Radius of the gas bubble R_{GB} ($= 37, 49, 62 \mu\text{m}$)
- Standoff distance from the laser focus to the proximal bubble interface d ($= 52, 67, 85 \mu\text{m}$)

We measure the probability of cavitation inception resulting from shock-bubble interaction for each parameter set (R_{GB} , d). The shock reflects at the bubble interface as a tension wave whose passage may in principle induce cavitation bubble nucleation in the gel between the laser focus and the preexisting bubble. The probability (out of 50 experimental runs) is judged based on whether nucleated bubbles are observed or not with the pixel size of $0.33 \mu\text{m}$ from the image recorded 20 ns after the shock collision at the bubble interface. Since structural damage in the gel will be caused by cavitation bubble nucleation, the gel sample with a newly created gas bubble is used for every shock-bubble-interaction experiment. We note that visible-sized (or microns-sized) impurities such as gas bubble nuclei or contaminant particles in the gel were not observed from the images. However, submicron-sized gas bubble nuclei will preexist in gelatin gels.²³ Since the local network of gel fibers is nonuniform with varying elasticity, the size and shape of bubble nuclei stabilized in gels can vary at different positions.²⁴

III. SIMULATION

A. Problem description

We simulate the experiment described in section II C and II D in order to investigate acoustic phenomena including the shock-bubble interaction and discuss the subsequent cavitation inception. The calculation domain is depicted, together with initial and boundary conditions, in Fig. 2

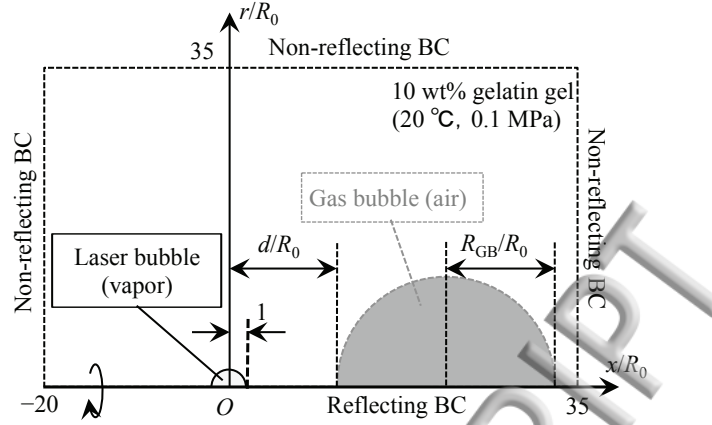


FIG. 2. Schematic of the initial configuration for the simulation.

where the coordinates are normalized by the initial radius R_0 of the laser-induced bubble. Now that the problem is axisymmetric about the x axis, we solve the domain $r \geq 0$ only.

B. Simulation model

Since the laser-induced shock pressure (on the order of 100 MPa to 1 GPa as will be seen Fig. 4(b)) is far larger than the gel elasticity ($E = 60$ kPa), we may model acoustic phenomena in the gel by the following multicomponent Euler equations for two-dimensional axisymmetric fluid flow (written in cylindrical coordinates):²⁵

$$\begin{pmatrix} \rho \\ \rho u \\ \rho v \\ e \end{pmatrix}_t + \begin{pmatrix} \rho u \\ \rho u^2 + p \\ \rho v v \\ (e + p)u \end{pmatrix}_x + \begin{pmatrix} \rho v \\ \rho u v \\ \rho v^2 \\ (e + p)v \end{pmatrix}_r + \frac{1}{r} \begin{pmatrix} \rho u \\ \rho u v \\ \rho v^2 \\ (e + p)v \end{pmatrix} = \mathbf{0}, \quad (1)$$

where ρ is density, u and v are velocity components, respectively, in the x and r coordinates, p is thermodynamic pressure, e is total energy (per unit volume), and the subscript denotes partial differentiation with respect to variable t , x , or r . Here, the effect of surface tension is assumed negligible and thus ignored.

The system of Eq. (1) is closed by the stiffened gas equation of state

$$\frac{p}{\gamma - 1} + \frac{\gamma P_\infty}{\gamma - 1} = e - \frac{\rho}{2} (u^2 + v^2) \quad (2)$$

TABLE I. Physical properties of the 10 wt% gelatin gel, water (liquid), air, and water (vapor) at standard temperature and pressure (20 °C and 1 atm).

Material	ρ (kg/m ³)	c_∞ (m/s)	γ (-)	P_∞ (GPa)	E (kPa)
10 wt% gel	1030	1553	6.72	0.37	60
Water (liquid)	1000	1450	6.12	0.34	N/A
Air	1.2	343	1.4	0	N/A
Water (vapor)	0.75	419	1.3	0	N/A

where γ and P_∞ represent, respectively, the stiffness and tensile strength of liquid-like materials. For (perfect) gases where no intermolecular force appears ($P_\infty = 0$), γ stands for the ratio of specific heats. It follows from Eq. (2) that the speed of sound is given by $c_\infty = \sqrt{\gamma(p + P_\infty)/\rho}$.²⁶ Table I summarizes the values of γ and P_∞ as well as other thermodynamic properties for materials of our concern (at standard temperature and pressure)^{27,28} and our measurement of the gel elasticity. For reference, we also document the values of (liquid-phase) water in this table, showing that the inclusion of 10 wt% gelatin in water leads to larger values of stiffness γ and tensile strength P_∞ .

The numerical method is based on the shock-interface capturing scheme proposed by Johnsen and Colonius, which allows us to stably simulate compressible fluid flow involving both shocks and material interfaces.²⁵ For spatial discretization, a fifth-order finite volume WENO scheme with the HLLC approximate Riemann solver is adopted. The time integration is handled by a third-order TVD Runge–Kutta scheme. The time step is uniform with maximum CFL number set below 0.1. The computational grid is based on two-dimensional Cartesian coordinates and uniform with grid spacing $\Delta x = \Delta r = 0.04R_0$, according to the simulation of Ando, Liu, and Ohl.¹⁶ The computational domain is taken to be large enough to eliminate solution contamination from spurious waves that may numerically arise from the non-reflecting boundary condition²⁹ (see Fig. 2). The simulation is performed with the initial plasma conditions¹⁶ of radius $R_0 = 6 \mu\text{m}$ and pressure $p_i = 1.9 \text{ GPa}$. These initial conditions were selected for the simulation to agree with the measured evolution of the shock front and the bubble wall.

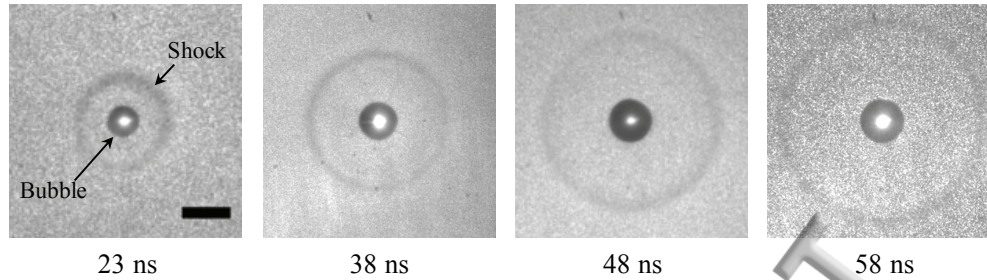


FIG. 3. Images of the laser-induced shock and bubble different times after the IR laser pulse focusing. The scale bar represents 50 μm .

IV. RESULTS AND DISCUSSION

A. Evolution of the laser-induced phenomena without bubble interaction

Figure 3 shows images of the shock and bubble different times after the IR laser pulse focusing; the shock is identified as a dark annulus and its front is defined as the midpoint of the annulus. It is confirmed that the shock propagates outward and the bubble behind the shock front grows due to initial high pressure of the laser-induced plasma. The visualization was repeated ten times for each recording time in order to calculate the average positions (and their standard deviations) of the shock front and bubble interface, which are plotted as a function of the time after the laser focusing; see Fig. 4(a) where the Euler flow simulation (section III) is also presented for comparison. The simulation is found to well reproduce the shock and bubble evolution. Furthermore, the spatial evolution of the simulated shock wave at different times after the laser focusing is presented in Fig. 4(b). Here, we note the possibility of having a strong tensile wave followed by a laser-induced shock wave in a gel whose elasticity is sufficiently large, as observed in the experiment of Brujan and Vogel.³⁰ However, the elasticity of our gel ($E = 60$ kPa) is lower than that of their polyacrylamide (PAA) gel ($E = 400$ kPa). This suggests that our gel concentration is so low that dissipation and elasticity in our gel do not play a major role in dynamics of the laser-induced shock and bubble.

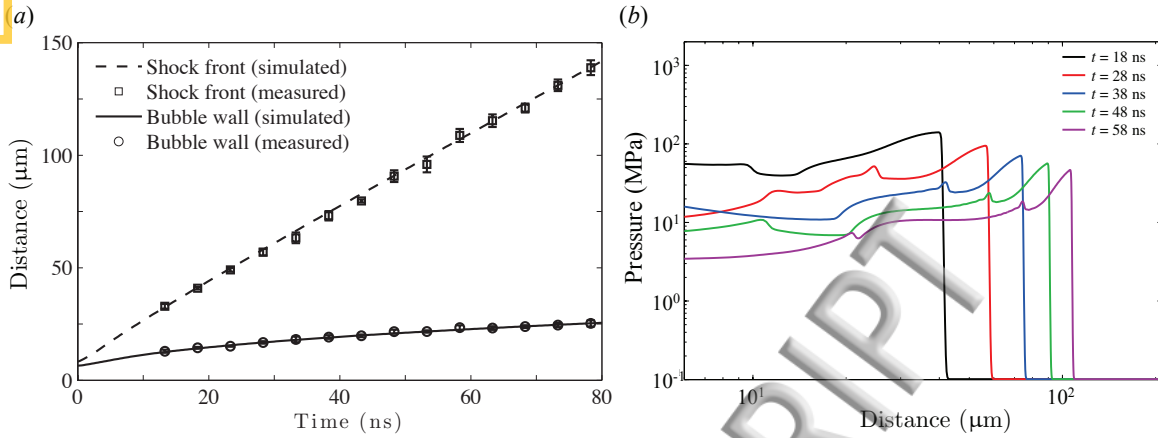


FIG. 4. (a) Temporal evolution of the shock front and the bubble wall. The error bar denotes the standard deviation out of 10 measurements. (b) Spatial evolution of the simulated shock wave different times after the IR laser focusing.

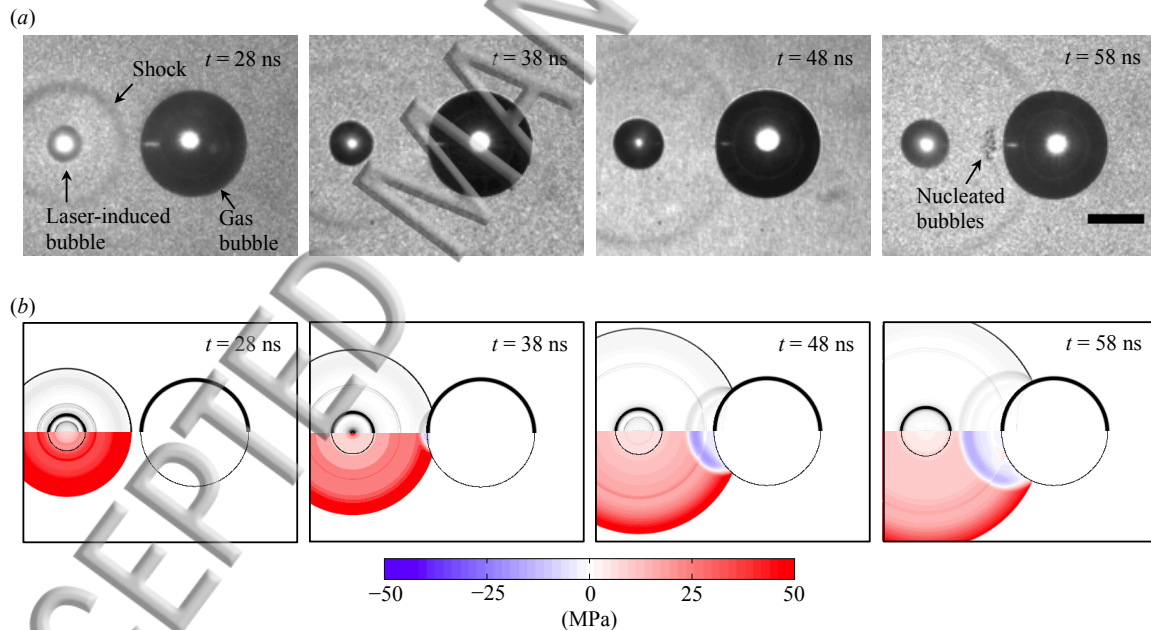


FIG. 5. Evolution of the shock-bubble interaction and its accompanying cavitation in the gel for $(d, R_{GB}) = (67 \mu\text{m}, 49 \mu\text{m})$. (a) Images from the experiment (the scale bar: $50 \mu\text{m}$). In this particular example, visible-sized cavitation bubbles nucleate, in frame 4, by shock-bubble interaction. (b) Evolution of the numerical Schlieren (top) and pressure distribution where the nominal interface location is depicted by black lines (bottom).

Shock-bubble interaction in the gel and the subsequent cavitation inception

We now examine shock-bubble interaction in the gel. As an example, we see the case of $(d, R_{GB}) = (67 \mu\text{m}, 49 \mu\text{m})$ in Fig. 5 that presents the measured and simulated evolution of the shock-bubble interaction; the numerical Schlieren²⁶ and pressure distribution corresponding to the experimental images are plotted for the simulation. It is confirmed that the simulation can well reproduce both the shock propagation and the bubble motion. In frame 1, the laser-induced shock propagates toward the preexisting gas bubble of $R_{GB} = 49 \mu\text{m}$. In frame 2, the shock wave collides with the bubble interface at the proximal side. In frame 3 (10 ns after the shock collision in frame 2), the reflected shock propagates, as a tension wave, back to the laser focus, generating a strong tension with negative pressure (at -24 MPa from the simulation) in the gel between the laser focus and the preexisting bubble. It is instructive to note that the gel temperature will change along an adiabat³¹, but the temperature drop after the tension wave passage is expected to be slight (within fraction of 1°C) so that the cavitation event is evaluated essentially at the room temperature. In this particular example, cavitation bubbles nucleate under this tension state and grow into visible size (on the order of a couple of microns), which is the definition of cavitation inception in this study, in frame 4 (10 ns after frame 3). We note that cavitation inception is a random event; (visible-sized) cavitation bubbles nucleate in some experiments (e.g., Fig. 5(a)) but do not appear in the others, even though the experimental parameters are fixed. To be more specific, the cavitation inception in our experiment will arise from stabilized gas bubble nuclei of submicron size²³ (i.e., heterogeneous cavitation inception). The size and shape of gas bubble nuclei will vary at different positions in the gel, depending on the local network of gel fibers with nonuniform elasticity.²⁴ As a result of randomness in the state of the cavitation nuclei, the heterogeneous cavitation inception becomes stochastic. In the following, the cavitation inception is to be analyzed statistically.

As explained in section II D, the visualization was repeated 50 times in each case of (d, R_{GB}) to define the cavitation inception probability that is summarized in Fig. 6. This data show a monotonic decrease in the probability as the standoff distance d increases, suggesting that the tension state obtained by the reflected shock is emphasized as the standoff distance decreases. The data also show a monotonic increase in the probability as the gas bubble radius R_{GB} increases. According to the classical nucleation theory^{9,32}, this trend may be explained by the fact that the stretched area by the reflected shock is augmented by increasing the bubble size so that cavitation becomes

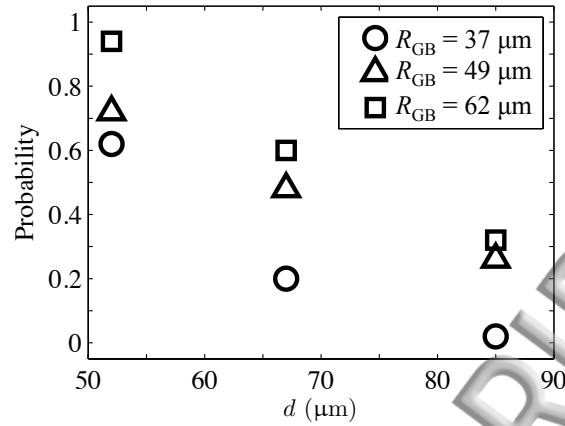


FIG. 6. The cavitation inception probability vs. standoff distance d and gas bubble radius R_{GB} .

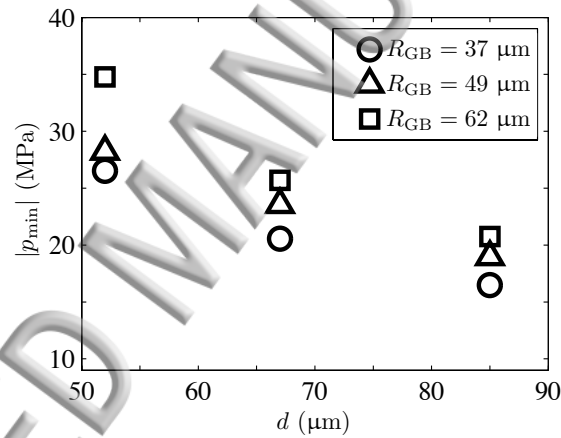


FIG. 7. The simulated minimum pressure $|p_{\min}|$ vs. standoff distance d and gas bubble radius R_{GB} .

more likely to occur.

To relate the cavitation inception probability to the tension state in the gel, we summarize (the absolute value of) the simulated minimum pressure $|p_{\min}|$ that is achieved after the reflection of the incident shock; see Fig. 7. The data show that the largest tension represented by $|p_{\min}|$ decreases as d increases or R_{GB} decreases, which is similar to the trend in the cavitation inception probability in Fig. 6. This suggests a strong correlation between the cavitation inception pressure and the largest tension; we combine Figs. 6 and 7 to plot the cavitation inception probability as a function of the minimum pressure; see Fig. 8. It is obvious that the cavitation inception probability increases as

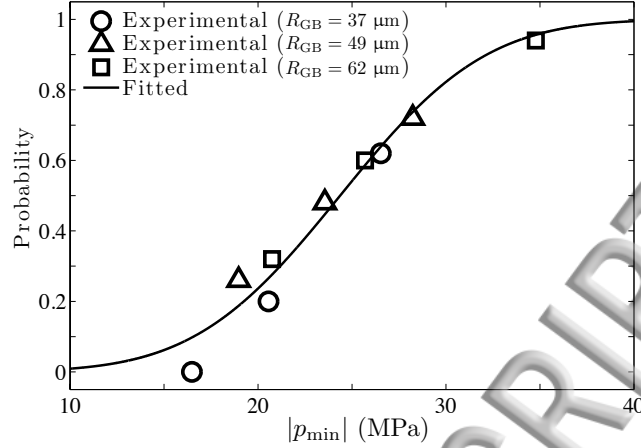


FIG. 8. The cavitation inception probability as a function of the minimum pressure $|p_{\min}|$. Each symbol (circle, triangle, or square) has three distinct points that correspond to the case of different standoff distance d ; the probability increases as d decreases.

the tension in the gel is emphasized.

From Fig. 8, we statistically define a threshold pressure for the cavitation inception. All the data points are fitted to the following sigmoid function:

$$P_{\text{cav}}(|p_{\min}|; |p_{\text{th}}|, \sigma) = \frac{1}{2} \left[1 + \text{erf} \left(\frac{|p_{\min}| - |p_{\text{th}}|}{\sqrt{2}\sigma} \right) \right], \quad (3)$$

where erf stands for the error function, p_{th} is the threshold pressure at which the probability is equal to one half (i.e., $P_{\text{cav}} = 0.5$), and σ is a deviation.¹¹ The fitting yields $p_{\text{th}} = -24.4$ MPa (and $\sigma = 6.2$ MPa). In comparison to the cavitation threshold pressure (-20.1 ± 3.4 MPa) from shock-bubble interaction in water¹⁷, that for the case of the 10 wt% gelatin gel is a bit more negative, meaning that the initial growth of submicron-sized bubble nuclei (under tension) to micron-sized cavitation bubbles is hindered by the gel viscoelasticity. Nonetheless, we may say that the gelatin concentration (10 wt%) is yet very low and the impact of the gel viscoelasticity on the nucleation dynamics is rather limited. However, even for the case of low concentration gelatin gels (as in our particular example), gel viscoelasticity will play a more important role in the later stage of inertial cavitation bubbles (such as collapse dynamics).^{30,33–37}

CONCLUSIONS

We experimentally and numerically investigated cavitation inception induced by shock-bubble interaction in a 10 wt% gelatin gel. An optical visualization technique based on nanosecond laser pulses at 532 nm and 1064 nm was used to observe interaction between a laser-induced shock and a preexisting gas bubble in the gel and its accompanying cavitation bubble nucleation; the cavitation inception probability was determined from the repeated experimental runs. To infer the pressure field in the shock-bubble interaction problem, the Euler flow simulation was performed and shown to agree with the measured evolution of the shock and bubble motion. It follows from a combination of the experiment and the simulation that the cavitation inception pressure in the gel is statistically predicted at -24.4 MPa (at which the cavitation inception probability is equal to one half) and turns out to be similar to that from shock-bubble interaction in water. This suggests that viscoelasticity of the 10 wt% gelatin gel has a limited impact on bubble nucleation dynamics.

ACKNOWLEDGEMENTS

We would like to thank Tomoki Kondo for his support to the simulation. We would also like to thank the anonymous referees for their insightful comments that enabled us to improve our paper. This study was supported by JSPS KAKENHI Grant Number 17H04905.

REFERENCES

- ¹M. R. Bailey, V. A. Khokhlova, O. A. Sapozhnikov, S. G. Kargl, and L. A. Crum. Physical mechanisms of the therapeutic effect of ultrasound (a review). *Acoustical Physics*, 49(4):369–388, 2003.
- ²M. R. Bailey, J. A. McAteer, Y. A. Pishchalnikov, Y. A. Hamilton, and T. Colonius. Progress in lithotripsy research. *Acoustics Today*, 2:18–29, 2006.
- ³T. G. Leighton and R. O. Cleveland. Lithotripsy. *Proc. Inst. Mech. Eng. H*, 224(3):317–342, 2010.
- ⁴C. E. Brennen. Cavitation in medicine. *Interface Focus*, 5:20150022, 2015.
- ⁵W. W. Roberts, T. L. Hall, K. Ives, J. S. Wolf Jr., J. B. Fowlkes, and C. A. Cain. Pulsed cavitation ultrasound: Anoninvasive technology for controlled tissue ablation (histotripsy) in the rabbit kidney. *J. Urol.*, 175(6):734–738, 2006.

- ⁶C. Coussios and A. R. Ronald. Applications of acoustics and cavitation to noninvasive therapy and drug delivery. *Annu. Rev. Fluid Mech.*, 40:395–420, 2008.
- ⁷P. Zhong, I. Cioanta, S. L. Zhu, F. H. Cocks, and G. M. Preminger. Effects of tissue constraint on shock wave-induced bubble expansion in vivo. *J. Acoust. Soc. Am.*, 104:3126–3129, 1998.
- ⁸S. Zhu, T. Dreyer and M. Liebler, R. Riedlinger, G. M. Preminger, and P. Zhong. Reduction of tissue injury in shock-wave lithotripsy by using an acoustic diode. *Ultrasound Med. Biol.*, 30:675–682, 2004.
- ⁹E. Herbert, S. Balibar, and F. Caupin. Cavitation pressure in water. *Phys. Rev. E*, 74:041603, 2006.
- ¹⁰A. D. Maxwell, T. Y. Wang, C. A. Cain, J. B. Fowlkes, O. A. Sapozhnikov, M. R. Bailey, and Z. Xu. Cavitation clouds created by shock scattering from bubbles during histotripsy. *J. Acoust. Soc. Am.*, 130:1888–1898, 2011.
- ¹¹A. D. Maxwell, C. A. Cain, T. L. Hall, J. B. Fowlkes, and Z. Xu. Probability of cavitation for single ultrasound pulses applied to tissues and tissue-mimicking materials. *Ultrasound Med. Biol.*, 130:449–465, 2013.
- ¹²E. Vlaisavljevich, K. W. Lin, A. Maxwell, M. Warnez, L. Mancina, R. Singh, A. Putnam, J. B. Fowlkes, E. Johnsen, C. Cain, and Z. Xu. Effects of ultrasound frequency and tissue stiffness on the histotripsy intrinsic threshold for cavitation. *Ultrasound Med. Biol.*, 41(6):1651–1667, 2015.
- ¹³E. Johnsen and T. Colonius. Shock-induced collapse of a gas bubble in shockwave lithotripsy. *J. Acoust. Soc. Am.*, 124(4):2011–2020, 2008.
- ¹⁴E. Johnsen and T. Colonius. Numerical simulations of non-spherical bubble collapse. *J. Fluid Mech.*, 629:231–262, 2009.
- ¹⁵C. D. Ohl and S. W. Ohl. *Shock wave interaction with single bubbles and bubble clouds*, volume 8 of *Shock Wave Science and Technology Reference Library*. Springer, 2013.
- ¹⁶K. Ando, A. Q. Liu, and C. D. Ohl. Homogeneous nucleation in water in microfluidic channels. *Phys. Rev. Lett.*, 109:044501, 2012.
- ¹⁷P. A. Quinto-Su and K. Ando. Nucleating bubble clouds with a pair of laser-induced shocks and bubbles. *J. Fluid Mech.*, 733:R3, 2013.
- ¹⁸S. A. Goss, R. L. Johnston, and F. Dunn. Comprehensive compilation of empirical ultrasonic properties of mammalian tissues. *J. Acoust. Soc. Am.*, 64:423–457, 1978.
- ¹⁹F. Hamaguchi and K. Ando. Linear oscillation of gas bubbles in a viscoelastic material under ultrasound irradiation. *Phys. Fluids*, 27:113103, 2015.

- ²⁰H. Kolsky. An investigation of the mechanical properties of materials at very high rates of loading. *Proc. Phys. Soc. B*, 62:676–700, 1949.
- ²¹A. Vogel, S. Busch, and U. Parlitz. Shock wave emission and cavitation bubble generation by picosecond and nanosecond optical breakdown in water. *J. Acoust. Soc. Am.*, 100:148–165, 1996.
- ²²A. Vogel. Nonlinear absorption: intraocular microsurgery and laser lithotripsy. *Phys. Med. Biol.*, 42(895):895–912, 1997.
- ²³D. Yount. Skins of varying permeability: A stabilization mechanism for gas cavitation nuclei. *J. Acoust. Soc. Am.*, 65:1429–1439, 1979.
- ²⁴W. Kang, A. Adnan, T. O’Shaughnessy, and A. Bagchi. Cavitation nucleation in gelatin: Experiment and mechanism. *Acta Biomater.*, 67:295–306, 2018.
- ²⁵E. Johnsen and T. Colonius. Implementation of WENO schemes in compressible multicomponent flow problems. *J. Comput. Phys.*, 219:715–732, 2006.
- ²⁶E. Johnsen. *Numerical simulations of non-spherical bubble collapse: With applications to shock-wave lithotripsy*. PhD thesis, California Institute of Technology, 2008.
- ²⁷V. Coralic and T. Colonius. Finite-volume weno scheme for viscous compressible multicomponent flows. *J. Comput. Phys.*, 274:95–121, 2014.
- ²⁸A. B. Gojani, K. Ohtani, K. Takayama, and S. H. R. Hosseini. Shock Hugoniot and equations of states of water, castor oil, and aqueous solutions of sodium chloride, sucrose and gelatin. *Shock Waves*, 26:63–68, 2016.
- ²⁹K. W. Thompson. Time dependent boundary conditions for hyperbolic systems. *J. Comput. Phys.*, 68(1–24), 1987.
- ³⁰E. A. Brujan and A. Vogel. Stress wave emission and cavitation bubble dynamics by nanosecond optical breakdown in a tissue phantom. *J. Fluid Mech.*, 558:281–308, 2006.
- ³¹K. Nagayama, Y. Mori, K. Shimada, and M. Nakahara. Shock Hugoniot compression curve for water up to 1 GPa by using a compressed gas gun. *J. Appl. Phys.*, 91:476–482, 2002.
- ³²C. E. Brennen. *Cavitation and Bubble Dynamics*. Cambridge University Press, 2013.
- ³³E. A. Brujan. *Cavitation in Non-Newtonian Fluids: With Biomedical and Bioengineering Applications*. Springer, 2011.
- ³⁴C. Hua and E. Johnsen. Nonlinear oscillations following the Rayleigh collapse of a gas bubble in a linear viscoelastic (tissue-like) medium. *Phys. Fluids*, 25:083101, 2013.

- ³⁵G. Gaudron, M. T. Warnez, and E. Johnsen. Bubble dynamics in a viscoelastic medium with nonlinear elasticity. *J. Fluid Mech.*, 766:54–75, 2015.
- ³⁶M. T. Warnez and E. Johnsen. Numerical modeling of bubble dynamics in viscoelastic media with relaxation. *Phys. Fluids*, 27:063103, 2015.
- ³⁷J. B. Estrada, C. Barajas, D. L. Henann, E. Johnsen, and C. Franck. High strain-rate soft material characterization via inertial cavitation. *J. Mech. Phys. Solids*, 112:291–317, 2018.

ACCEPTED MANUSCRIPT